



# Heat flux measurements of turbulent and transitional 3D shock-boundary layer interactions generated by a single fin on a flat plate

Wieland Lühder, Erich Schülein<sup>2</sup>

#### **Abstract**

The three-dimensional shock wave boundary layer interaction in the vicinity of a single fin on a flat plate was investigated at Mach 3 and Mach 5 in the *Rohrwindkanal Göttingen*, a Ludwieg tube facility. Quantitative InfraRed Thermography (QIRT) was used to measure the spatial distribution of heat flux density in the interaction area on the flat plate. Under constant inflow conditions, the intensity of the generated shock wave could be precisely adjusted by aligning the shock generator. This made it possible to verify and refine the scaling laws for maximum heat loads induced along the attachment line in turbulent SWBLI. Further experiments on transitional shock-boundary layer interaction were used to investigate the quasiconical symmetry of the heat flux distribution, that emerge after adequate scaling. For this, a virtual, undisturbed boundary layer that starts at the leading edge of the fin is taken as reference. The maximum heat load depends on the initial boundary layer state at the separation location and can be linearly scaled, using only the transition onset and end location.

Keywords: shock-boundary layer interaction, Stanton number, quasiconical, turbulent, transitional

#### **Nomenclature**

Latin

 $M\,$  – Mach number

P – pressure

 $Re_1$  – unit Reynolds number

 $Re_x$  - Reynolds number based on chord length

r – leading edge radius of the fin or recovery factor

St – Stanton number

 $St_1$  – reference Stanton number in the undisturbed boundary layer

T – Temperature

x,y,z – coordinates in the wind tunnel system

x', y', z' - rotated coordinates

 $x_{tr}$  – location of transition onset

Greek

 $\beta$  – fin angle

 $\theta$  – conical angle

 $\xi$  – shock intensity

ζ – boundary layer state parameter

Superscripts

+ - Value at the reattachment line

Subscripts

0 – stagnation conditions

2 – conditions downstream of the shock

 $\infty\,$  –  $\,$  free stream conditions

fin - respective to the fin leading edge

Plateau – constant value within the quasiconical symmetry

Plexi - material properties of plexiglas

VD - calculated using the Van Driest II relation

w - wall conditions

## 1. Introduction

Predicting shock-wave boundary layer interactions (SBLI) are still one of the most challenging aspects of designing hypersonic vehicles. The effect of the flow onto the model within SBLI vastly exceeds those of hypersonic boundary layer flow without the effects of SBLI. In particular, the exact knowledge of wall pressure is relevant for rudder efficiency and the increased thermal load sets difficult conditions for the

<sup>&</sup>lt;sup>1</sup>DLR Göttingen, Department of High Speed Configurations, Institute of Aerodynamics and Flow Technology, wieland.luehder@dlr.de

<sup>&</sup>lt;sup>2</sup>DLR Göttingen, Department of High Speed Configurations, Institute of Aerodynamics and Flow Technology

heat shield and material properties. For high-quality vehicle design, a precise prediction of those crucial design part is required, but currently not available for flows with SBLI. Numerical simulations often fail to accurately model SBLI [1] and there is still a lack of systematic experimental data and parameter studies on thermal loads to reliably test scaling approaches [2].

It is well known that a sufficiently strong shock-induced pressure increase within the boundary layer can cause flow separation and laminar-turbulent transition. The boundary layer's susceptibility to separation, the size of the interaction area and the induced aerothermal loads vary greatly with laminar-turbulent transition, making the study of transitional SBLI particularly interesting.

To break down this complex problem of 3D SBLI into solvable tasks, several canonical configurations [3] are of particular interest for basic SBLI research. The geometry of choice for this study is a single fin on a flat plate, which is relevant for corner flows, such as rudders, fins and engine inlets. It is particular suitable for parameter studies, as the boundary layer state and the shock intensity can be separately tuned. The typical flow topology of the single fin on a flat plate with a turbulent SBLI (STBLI) is displayed in Fig. 1, showing the wall pressure at the flat plate (green-yellow scale) and the cross flow velocity in a volume slice (rainbow scale). In the latter, one can see the shock front and the separation vortex. The maximum pressure on the wall is reached near the flow's reattachment line, and the upstream influence line is the dividing line between the interaction zone and the undisturbed boundary layer. The entire interaction area exhibits quasi-conical symmetry, with the virtual conical origin (VCO) located slightly upstream of the leading edge of the fin. Exceptions from this symmetry are the *inception region* near the leading edge and downstream the effects of a finite fin geometry. Within the valid area of this symmetry, the flow and surface parameters solely depend on the conical angle  $\theta$  and little on the streamwise coordinates x (wind tunnel reference frame) or x' (rotated reference frame of the fin).

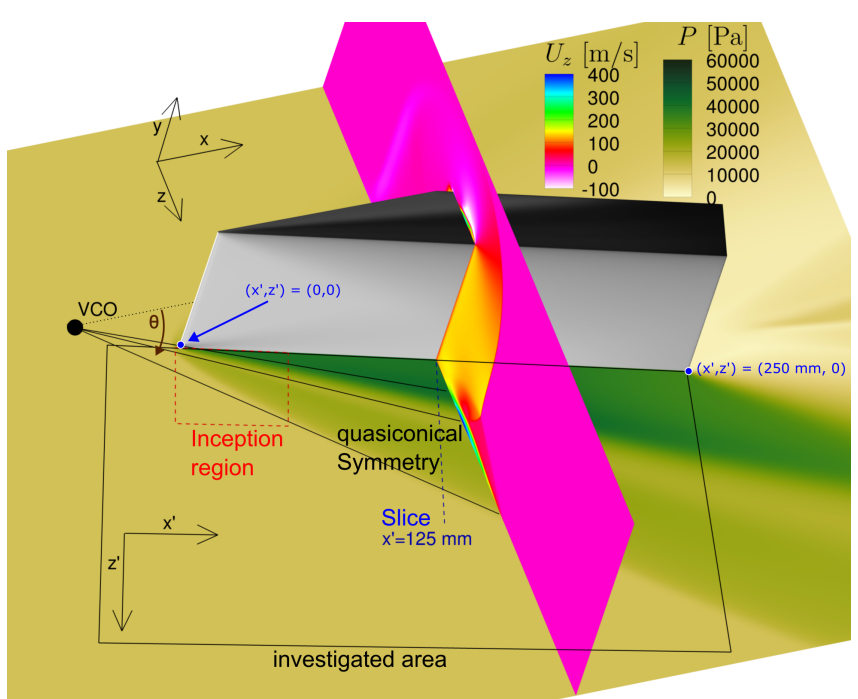


**Fig 1.** 3D RANS simulation of the model geometry at a Mach number of M=3 and a fin angle of  $\beta=20^{\circ}$ . The yellow-green colour scale represents the surface pressure of the flat plate and the rainbow scale is the crossflow air velocity at one slice. Additionally, the VCO, the inception region, the conical angle  $\theta$  and the rotated coordinate system (x',z') are sketched [4].

This study used quantitative infrared thermography (QIRT) to measure heat flux density distributions. QIRT involves using an infrared camera to detect changes in surface temperature over time. In contrast

to other experimental temperature measurement techniques, this camera can be easily calibrated and the temperature data can be directly processed to obtain the dimensionless Stanton number. With this setup, the 2D surface data of dimensionless heat flux was obtained for a large range of configurations with fin angles from  $\beta=2^\circ$  to  $\beta=32^\circ$ , Mach numbers of M=3 and M=5 and various Unit Reynolds numbers  $Re_1$  of the flow. These are then used to derive scaling laws to model the maximum heat flux at the reattachment line. The aim of this study is to investigate how these laws depend on shock intensity and boundary layer state, and to determine the scaling required to fit the downstream decreasing value of the heat flux into the theory of quasiconical symmetry.

# 2. Experimental techniques

## 2.1. Wind tunnel, experimental model and test matrix

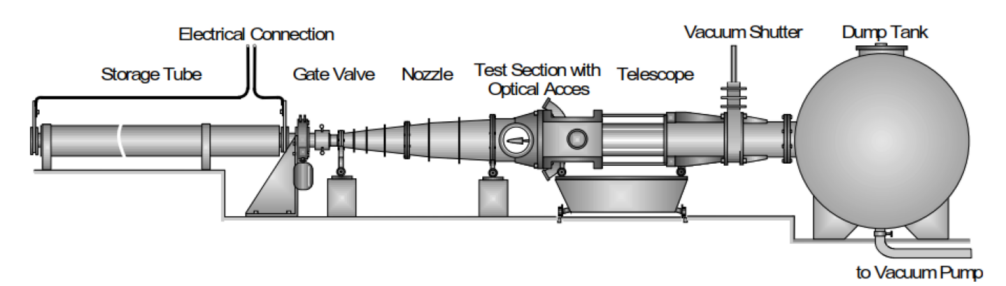


Fig 2. Sketch of the Rohrwindkanal Göttingen (RWG) [2].

The experimental investigations were conducted in the *Rohrwindkanal Göttingen* (RWG)[5], which is a Ludwieg tube facility located in the DLR Göttingen. The relevant components and their arrangement can be seen in Fig. 2, where the gate valve separates the pressurized storage tube of 80 m length from the evacuated test section and dump tank. The test section has a cross section of  $0.5 \times 0.5$  m and the maximum run time reaches about 0.3 s, limited by the length of the storage tube. During this time, the stagnation temperature and pressure and thus the unit Reynolds number  $Re_1$  of the flow stays nearly constant.

Different combinations of pressurized storage tubes (ambient temperature or heated) and Laval Nozzles cover Mach numbers from  $2 \le M \le 7$  and a wide range of achievable unit Reynolds numbers [5, 2]. For this study, Mach numbers of M=3 and M=5 were selected with  $Re_1=45\cdot 10^6\,\mathrm{m}^{-1}$  for most of the test runs. For a set of experiments with a transitional boundary layer at M=3, the natural transition location  $x_{tr}$  was varied by altering the pressure in the storage tube. Thereby the unit Reynolds number was tuned between  $15\cdot 10^6\,\mathrm{m}^{-1}$  and  $58\cdot 10^6\,\mathrm{m}^{-1}$ . A summary of the flow conditions and resulting transition onset locations  $x_{tr}$  is provided in Table 1.

The investigated model geometry is a single fin on a flat plate, sketched in Fig. 3. The fin can be exchanged to adjust the leading edge bluntness, ranging from a sharp fin to a fin with a nose radius of r=0.8 mm. Using a rotatable insert within the flat plate, the fin angle  $\beta$  respective to the free stream can be continuously adjusted. Values between  $\beta=2^\circ$  and  $\beta=32^\circ$  were used within this study. Like indicated in Fig. 3, the distance between the flat plate leading edge and the center of rotation is 374.4 mm, leaving enough space for a fully turbulent boundary layer to develop. As this insert is located

**Table 1.** Averaged flow parameters investigated in the present study for experiments with a turbulent boundary layer and parameter range for transitional measurements.

М	boundary layer state	$Re_1$ (10 <sup>6</sup> m <sup>-1</sup> )	<i>T</i> <sub>0</sub> (K)	$T_{\infty}$ (K)	$P_0$ (10 $^5$ Pa)	$x_{tr}$ (mm)
3	turbulent	45.0(5)	254(6)	91(2)	4.67(16)	45
3	transitional	15-58	264(4)	94(2)	1.7-6.5	30-130
5	turbulent	45.0(5)	400(4)	66.6(6)	24.8(4)	110

off-center in the flat plate, a 180 degrees flip of the flat plate allowed to reduce this distance to 185.6 mm or  $x_0=70.5$  mm as a distance between the leading edges of the plate an fin at  $\beta=20^{\circ}$ .

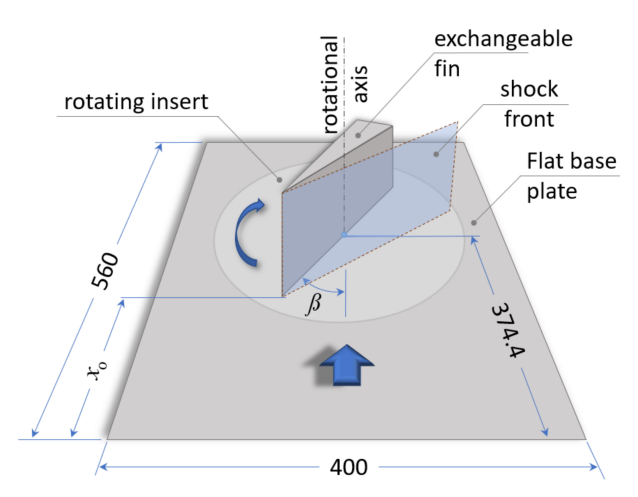


**Fig 3.** Wind tunnel model geometry with the flat plat, the rotatable insert and the exchangeable fin for the turbulent case with an indicated length of 374.4 mm from the leading edge to the rotational axis. All lengths are given im mm.

#### 2.2. Quantitative Infrared Thermography (QIRT)

For temperature measurements with QIRT, the rotating insert of the model is made of Plexiglas. With a low specific heat capacity  $c_{P,Plexi}=1,48~{}^{1}/{}_{kgK}$  and low thermal conductivity  $\lambda_{Plexi}=0,202~{}^{W}/{}_{km}$ , the observed temperature differences during one short wind tunnel run are far larger than on a steel surface. Due to this, a grid of metallic markers within the surface is easily visible and used for image rectification. The images were taken with an IRCAM EQUUS 327kl infrared camera, that features a resolution of  $640\times512$  pixel and a frame rate of 105 images per second. It was mounted on the outside of a 300 mm diameter Germanium window, using a germanium objective with a focal length of 50 mm. This camera was already often used in this wind tunnel [6, 7, 8, 4] and the necessary calibration and image processing steps best described in [6].

From the obtained wall temperatures  $T_i$  at time i, the heat flux  $\dot{q}_w$  was calculated by applying the integration procedure from Cook and Feldermann (see [9] Eq. 83 or [6]) to the data of each pixel:

$$\dot{q}_w(t_n) = 2\sqrt{\frac{\rho_{Plexi}c_{P,Plexi}\lambda_{Plexi}}{\pi}} \cdot \left[\sum_{i=1}^n \frac{T_i - T_{i-1}}{\sqrt{t_n - t_i} + \sqrt{t_n - t_i - 1}}\right]$$
(1)

Using a fit of the resulting heat flux over the difference between the adiabatic flow temperature  $T_{ad}$  and the measured temperature of the wall  $T_w$ , the average Stanton number was calculated with the stagnation flow conditions [10]

$$St = \frac{\dot{q}}{\rho_{\infty} u_{\infty} c_P (T_{ad} - T_w)} \,. \tag{2}$$

With the limited measurement time of the RWG, the adiabatic wall temperature  $T_{ad}$  cannot be measured experimentally and extrapolation from the available heat flux data is infeasible [4]. To determine the adiabatic temperature, the common recovery factor of r=0.89 was assumed, as is customary for turbulent boundary layers [10, 11]. Although this assumption is not strictly accurate for transitional flows or flows with SBLI in general, it provides a clear basis for normalising and presenting measurement results consistently outside these ranges.

For the configuration with M=3 and  $\beta=20^{\circ}$ , the resulting spatioal distribution of St is shown in Fig. 4. Here, the rotated reference frame of the fin is used, with the leading edge being at (0,0).

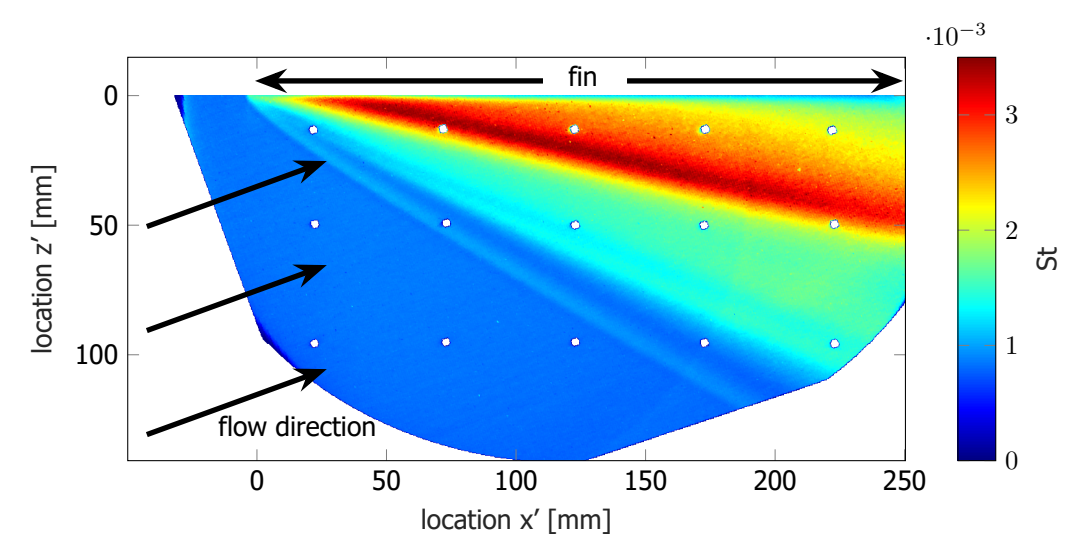


**Fig 4.** Spatial distribution of the measured Stanton number distribution at M=3 and  $\beta=20^{\circ}$ , rotated to the reference frame of the fin (x',z'). The white dots are at the locations of surface markers for photogrammetry processing.

#### 3. Results and discussion

#### 3.1. Quasiconical symmetry

As stated before and also visible in the 2D surface data in Fig. 4, the flow field of a single fin on a flat plate features a quasiconical symmetry. In a perfect symmetry, all relevant rays characterizing the separation vortex would intersect in the VCO. However, as previously noted in references [12, 13], this does not apply unconditionally to experimental data. In fact, reference [2] suggests that there are several different origins, depending on the variables and measurement locations of interest. For this data set, a suitable definition is the intersection of the inviscid shock plane of the fin with the Upstream influence line of the separation bubble on the flat plate (see Fig. 1). For Fig. 4, this would be at the coordinates (x',z')=(-39,-12) mm. In the conical coordinate system  $(\theta,x)$ , all measured values strongly depend on the conical angle but very little on the chordwise length [3, 14, 2]. That is why two

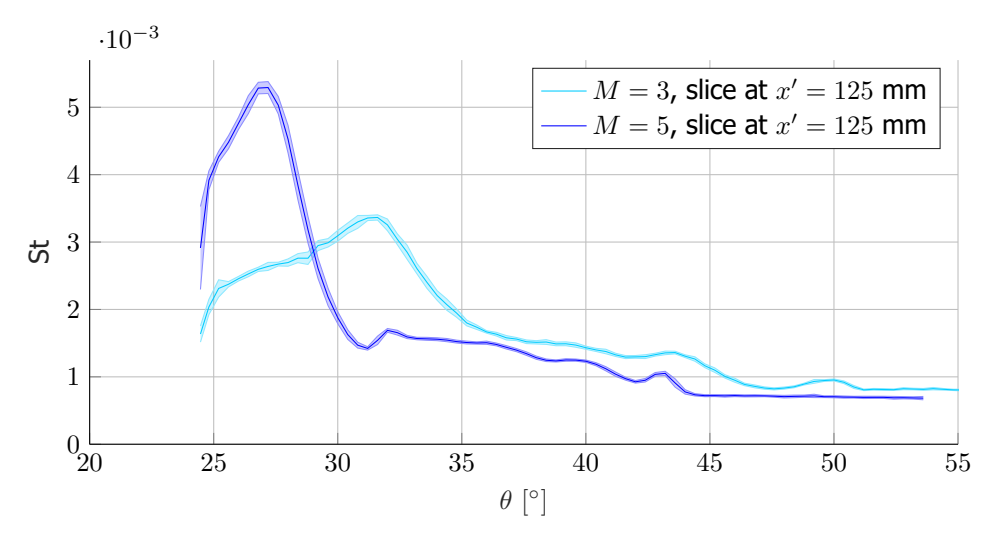


**Fig 5.** Slices of the Stanton number for the sharp fin at  $\beta=20^{\circ}$  for the Mach numbers M=3 and M=5 in conical representation over the conical angle  $\theta$ .

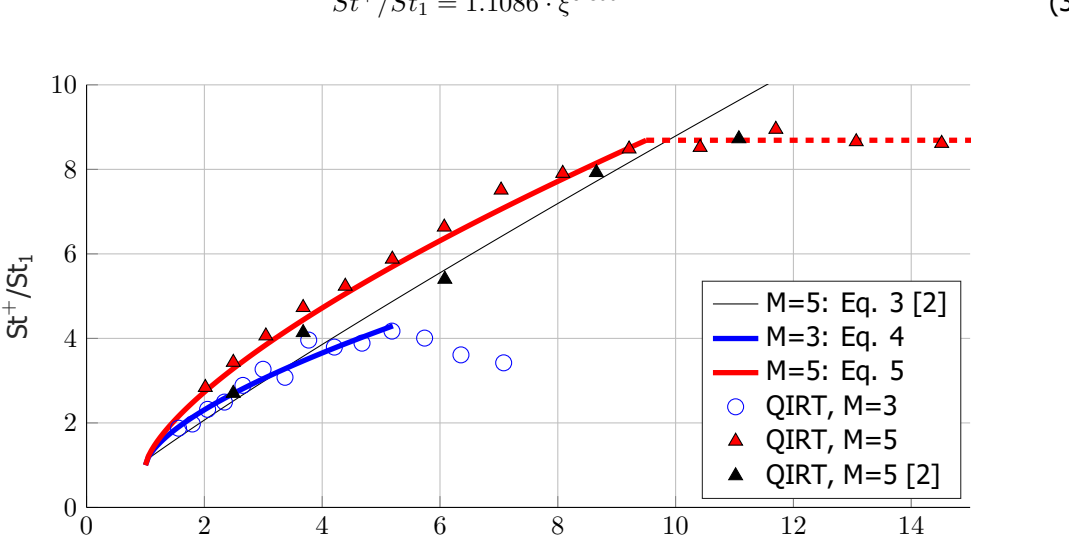
forms of data representation are commonly used: A slice of data perpendicular to the fin surface, with the data plotted against the conical angle  $\theta$  or conical rays along constant values of  $\theta$ . Fig. 5 shows the sliced Stanton number distribution for two investigated configurations at different Mach numbers.

Due to the location of the VCO, the first data points near the wall are at an angle of  $\theta \approx 24^{\circ}$ . From there, the measured Stanton number quickly rises towards its maximum  $St^+$  at the reattachment line. The following decrease below the separation vortex and several local maxima are the parts of the flow field, that are the hardest to reproduce in numerical simulations [1]. This is both a relevant and interesting topic, but not within the scope of this study. Beyond the separation line, which is at the last local maximum, the data reaches a constant value which is the Stanton number  $St_1$  of the undisturbed boundary layer.

Out of those slices,  $St^+$  was extracted for various chordwise locations of the slice. This yields a curve  $St^+(x)$ , which should display a constant value according to the concept of conical symmetry, except for the inception region near the leading edge of the fin [13]. This was often successfully demonstrated for pressure measurements [15, 13, 3]. In contrast to this presumably symmetrical flow field, explicit decrease in heat flux in downstream direction was mentioned in [2] and could be reproduced with the current experimental data on STBLI. This behavior is analyzed in more detail in the following section on transitional flow.

# 3.2. Turbulent shock-boundary layer interaction

For the turbulent SBLI (STBLI), the maximum Stanton number  $St^+$  was extracted and analysed at x'=125 mm. This location in the middle of the fin ensured the measurement point to be within the region of quasiconical symmetry. For each combination of Mach number and fin angle  $\beta$ ,  $St^+$  is normalized by the experimental Stanton number of the undisturbed boundary layer  $St_1$  of that specific wind tunnel run and plotted against the shock intensity  $\xi = P_2/P_\infty$  in Fig. 6. In an earlier study, Schülein [2] proposed an approximation (black line) for the scaled Stanton number along the reattachment line, which was based on his own experimental data (black triangles):



$$St^+/St_1 = 1.1086 \cdot \xi^{0.8992}$$
 (3)

Fig 6. Scaling of the normalized Stanton number at the reattachment line over the shock intensity for the two investigated Mach numbers. Previous data and Eq. 3 [2] are displayed in red.

 $\xi = P_2/P_{\infty}$ 

Current measurements at Mach 5 (red triangles) confirm the global trend observed in [2], and also clarify the empirical dependence of the normalised peak load on shock strength. At a fin angle of around  $\beta =$  $26^{\circ}$  ( $\xi = 9.5$ –10), saturation is clearly visible along the path. It appears that the finite height and length of the fin influence the large-scale 3D separation; strictly speaking, the conical symmetry is no longer present. In quantitative terms, the experimental data for the two investigated Mach numbers show slightly different trends and cannot be combined within the selected parameter space. The resulting fit, containing both the old and new data sets, provides the two displayed curves:

$$M = 3: St^{+}/St_{1} = 1 + 1.31 \cdot (\xi - 1)^{0.643}$$
(4)

$$M = 5: St^{+}/St_{1} = 1 + 1.73 \cdot (\xi - 1)^{0.697}$$
(5)

#### 3.3. Transitional SBLI

In order to analyse transitional SBLI, it is first necessary to understand the behaviour of the undisturbed transitional boundary layer in the wind tunnel. For this, the flat plate was investigated without having any fin mounted. To account for surface imperfections, flow inhomogeneities and other experimental uncertainties, the calculated Stanton number distribution was averaged in spanwise direction and plotted in Fig. 7 (left) against the distance to the leading edge x. The error bars quantify the standard deviation of all data points with the same coordinate  $\pm 1$  mm. A common display of transitional boundary layer data is the scaling of the running length with the unit Reynolds number,  $Re_x = Re_1 \cdot x$ . In Fig. 7 (right), all curves collapse onto similar shapes and show nearly identical values of  $Re_x$  for both the transition onset at the minimum values as well as the transition end at the maximum Stanton number. The black line is calculated with the empirical formula of Van Driest [7, 16] for undisturbed turbulent boundary layers, combined with the Reynolds analogy [10] to obtain the heat flux from the Skin friction coefficient in a rudimentary approximation. An overshoot in heat flux at the end of the transition location is normal and expected for transitional boundary layers [10]. Downstream of the transition, the experimental curves approach the Van Driest relation  $St_{VD}(Re_x)$  fairly well. Due to this agreement, the Van Driest curve was used as reference value to normalize the Stanton number in transitional SBLI.

Figure 8 shows the 2D Stanton number distribution of the fin at  $\beta=20^\circ$  and M=3 at four different values of  $Re_1$ . One can see the laminar boundary layer (black) and its natural transition to a turbulent boundary layer outside of the interaction region. This location is marked with a small arrow and moves upstream with increasing  $Re_1$ , as already shown in Fig. 7. Within the interaction, the reattachment line can be seen with the highest Stanton numbers measured, whereas the magnitude also depends on  $Re_1$ . Furthermore, within the turbulent part of the flow there is a clear upstream influence line visible

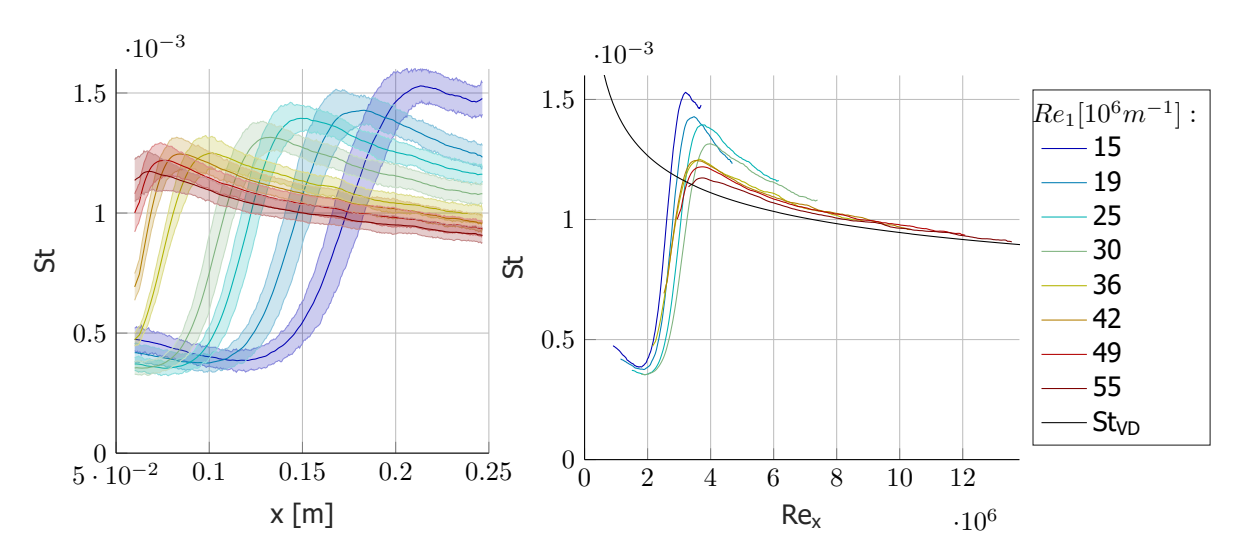


**Fig 7.** Spanwise averaged heat flux measurement on the flat plate without any fin, plotted against the distance to the leading edge (left) or the Reynolds number  $Re_x$  (right). The Unit Reynolds number of the incoming flow in  $10^6 {\rm m}^{-1}$  is indicated in the legend.

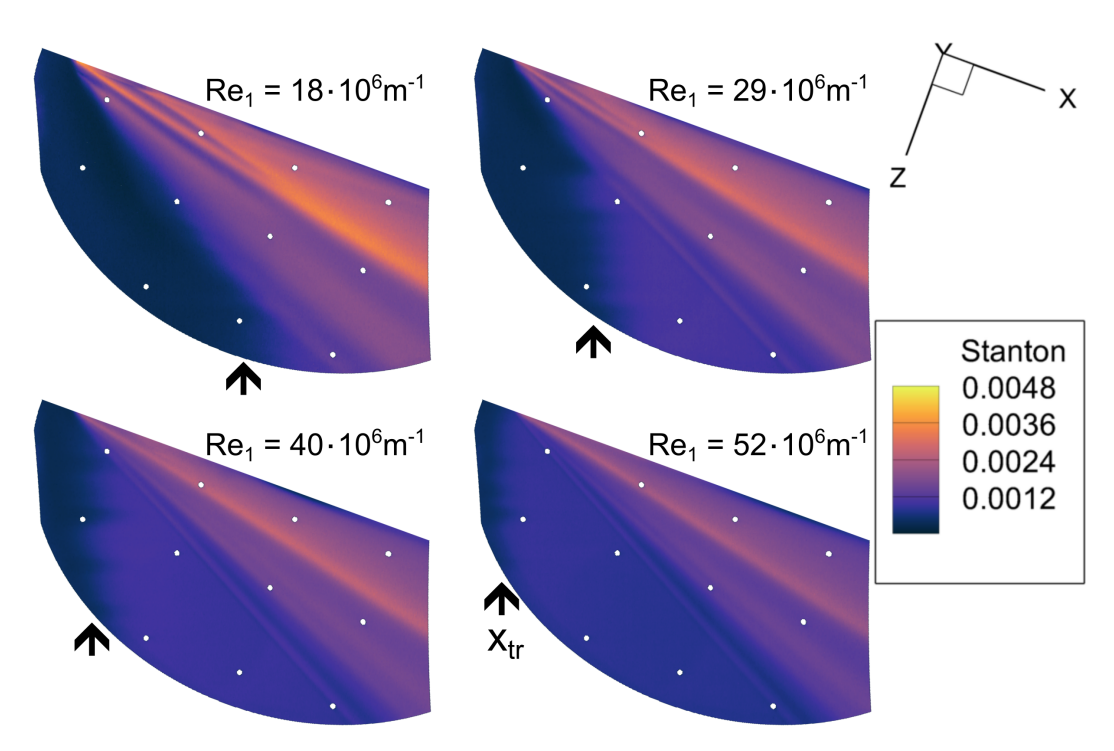


**Fig 8.** 2D images of the resulting Stanton number after processing the raw temperature images series with the *Heatfit* program. Displayed is the SBLI of the fin with  $\beta=20^{\circ}$  at various unit Reynolds numbers which yield in different natural transition locations  $x_{tr}$ , marked with a small arrow on each picture.

as a conical ray from the VCO. In the laminar parts, this line seems to blur out and there is a smooth transition from the undisturbed boundary layer to the interaction region. Last, within the inception region and for the configurations with the longest laminar running length, additional structures near the reattachment line become visible that are not of conical origin. The details of the flow there are complex and strongly related to the laminar-turbulent transition in the incoming boundary layer. They definitely require further in-depth investigation and will not be considered further here.

In Fig. 9, the measured values of  $St^+$  are presented, depending on the streamwise position  $Re_x$ . Lower unit Reynolds numbers of the flow result in higher heat flux and as expected from the turbulent case and previous studies [2, 7], the Stanton number drops off further downstream. The main focus of this study is to find a suitable scaling for those curves.

As the separation vortex starts at the leading edge of the fin, it is reasonable to scale the measured heat flux within this vortex with the values of a hypothetical new boundary layer starting from this point. This means, for a calculation of  $Re_x$ , the distance  $x_{fin}=x-70.5$  mm is used. Furthermore, the shock alters the free stream flow properties and results in a new unit Reynolds number  $Re_{1,2}$  of the flow downstream of the shock (without considering the SBLI). The reference heat flux within this new boundary layer cannot be experimentally measured, but is instead modeled with the Van Driest curve due to the excellent accordance previously shown. The result, named  $St_{undisturbedVD}(x_{fin})$ , is used in Fig. 10 to normalize the measured  $St^+$ , rather than the line in Fig. 7, which started at the leading edge of the flat plate.

Using those scaling approaches, several major observations become visible in Fig. 10. First, the decay of heat flux in streamwise direction could be completely compensated, such that the ratio of the measured Stanton number to the (shortened) reference boundary layer curve yields a constant value for each experiment. Thus the observed violation of quasiconical symmetry can be solved to be a consequence of boundary layer growth. Furthermore, it becomes even more evident, why so far only the

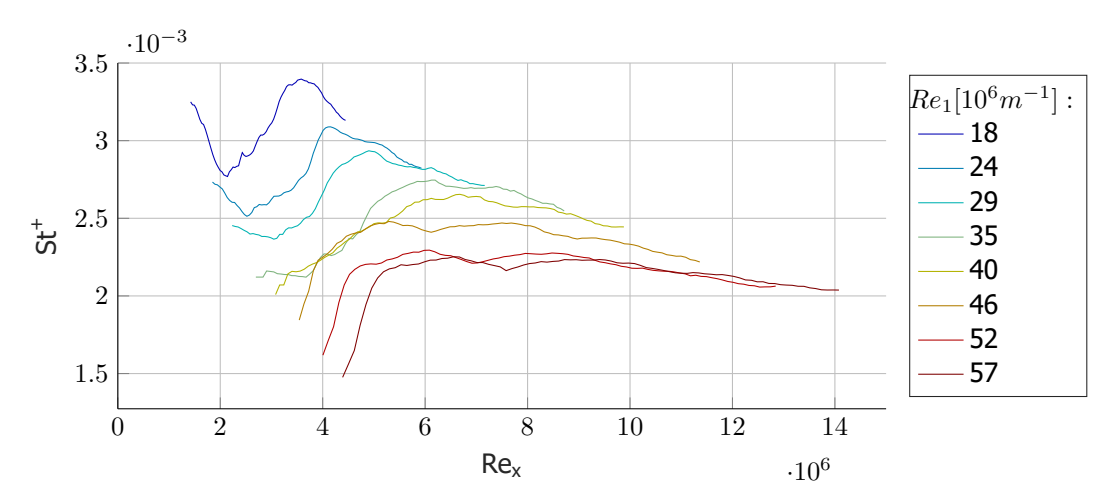


**Fig 9.** Raw data of the calculated Stanton number at the reattachment line  $St^+$  over  $Re_x$  for all investigated unit Reynolds numbers at M=3 and  $\beta=20^\circ$ .

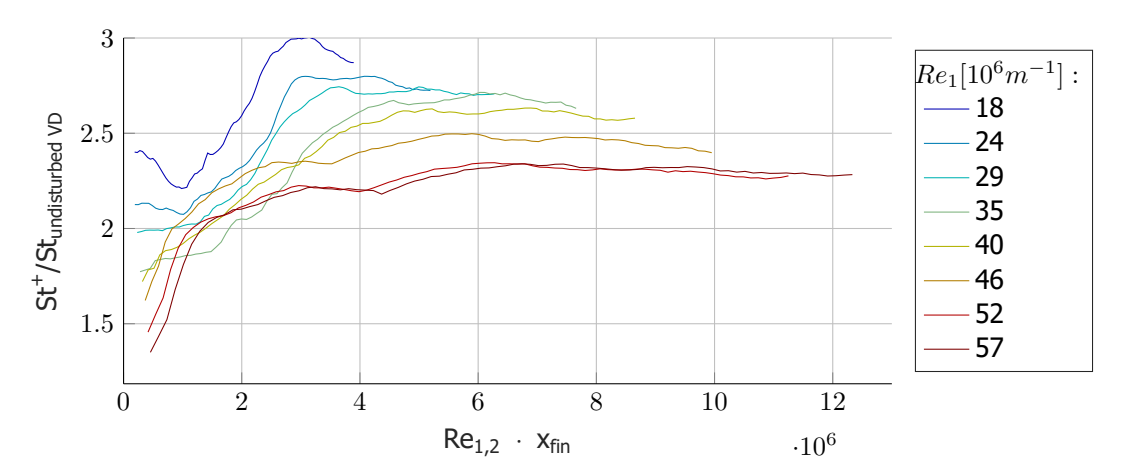


**Fig 10.** Measured Stanton numbers  $St^+$  at the reattachment line of the sharp fin at M=3 and  $\beta=20^\circ$ , with the magnitude and position scaled with a virtual boundary layer that starts at the fin leading edge.

pressure measurements provided constant results along conical rays, as the reference pressure within the reference turbulent boundary layer changes very little. As a second observation, the steep rise in heat flux now occurs at very similar values of  $Re_{xfin}$ . These data, as well as the data of the undisturbed boundary layer in Fig. 7 are not precise enough to derive exact statements of the transition effects within the separation vortex. They can not be distinguished from effects of the inception region in the turbulent boundary layer using OIRT measurements only.

The third feature of the scaled curves are the staggered plateau values, that are higher at lower values of  $Re_1$ . This suits the general statement, that SBLI are stronger in laminar boundary layers than in turbulent ones, but this behavior seems to be a continuous process in transitional boundary layers. To quantify the boundary layer state, the parameter

$$\zeta = \frac{Re_x - Re_{x,tr-on}}{Re_{x,tr-end} - Re_{x,tr-on}} \tag{6}$$

scales the streamwise Reynolds number  $Re_x$  with the transition onset and end locations  $Re_{x,tr-on}$  and  $Re_{x,tr-end}$  [17]. To obtain these, the locations of minimum and maximum Stanton number values from Fig. 7 were measured [6]. For all curves, where either one of those locations was outside of

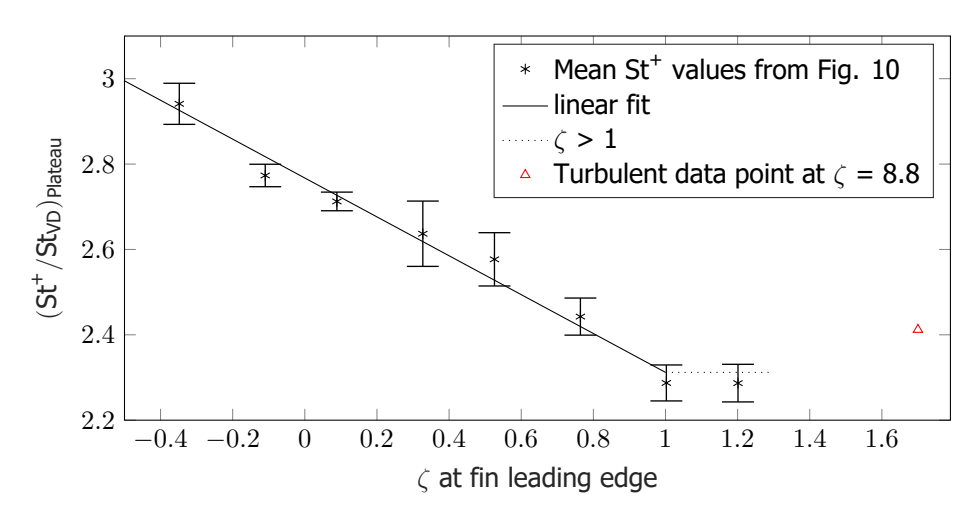


**Fig 11.** Normalized Stanton number ratio within the quasiconical symmetry, plotted against the boundary layer state parameter  $\zeta$  at the location of the leading edge of the fin for M=3 and  $\beta=20^\circ$ . The turbulent measurement point at  $\zeta\approx 8.8$  at the same shock intensity is displayed closer to the transitional data for visibility purposes.

the measured area, the transitional length  $Re_{x,tr-end} - Re_{x,tr-on}$  was set to the average value of the available curves.

Equation 6 yields  $\zeta<0$  for a laminar boundary layer and  $\zeta>1$  for a position  $Re_x$  in the turbulent part of the boundary layer. As the calculated Stanton number ratio respective to the new boundary layer depends on the boundary layer state, the value of the parameter  $\zeta$  at the start of the interaction, e.g. the fin leading edge is of significant interest. In Fig. 11,  $\zeta$  was calculated for all conducted experiments from Fig. 10, and the plateau of the Stanton number ratio within the quasiconical symmetry  $(St^+/St_{VD})_{Plateau}$  taken as average value of the given plots after reaching the near-constant part of the curve.

The calculated ratio in Fig. 11 shows a linear dependency on the boundary layer state parameter  $\zeta$ . This continues for laminar boundary layers ( $\zeta < 0$ ), but stops once a complately turbulent state is reached ( $\zeta = 1$ ). This means, the emerging boundary layer instablilties before the transition onset already affect its susceptibility to separation and its reaction to SBLI effects. For the one investigated shock intensity, the linear fit yields

$$(St^+/St_{VD})_{Plateau} = 2.312 \cdot (1 + 0.455 \cdot (1 - \zeta))$$
 for  $\zeta \le 1$  (7)

This data set can be expanded by the previous measurements with turbulent boundary layers. Without having exact data of the transition location available,  $\zeta \approx 8.8$  can be approximately assumed. For this, the relevant shock intensity was inserted into Eq. 4 to calculate the Stanton number ratio. But remember that in the section of STBLI, the values were scaled by one experimental point within the undisturbed boundary layer of the flat plate. If it is instead scaled by the shortened boundary layer to match the transitional post processing, one obtains a value (red triangle in Fig. 11) that is very similar to those at  $\zeta \geq 1$  in the transitional boundary layer. This suggests, that  $(St^+/St_{VD})_{Plateau}$  does not decrease any more for  $\zeta > 1$ , but only 2 data points are not to propose a systematic trend.

With the same scaling, the experimental data obtained while using the blunt fin geometries (r=0.8 mm) is presented in Fig. 12. The steep increase in heat flux is located at lower  $Re_{xfin}$ , but still at similar positions for all investigated unit Reynolds numbers. The major difference to the result of the sharp fins is a secondary increase in heat flux downstream of this alleged transition location. This is a geometrical feature that starts at a distance of x=130 mm from the fin leading edge and ends at x=171 mm,

independent of the Unit Reynolds number of the test run, and is probably linked to the detached shock geometry.

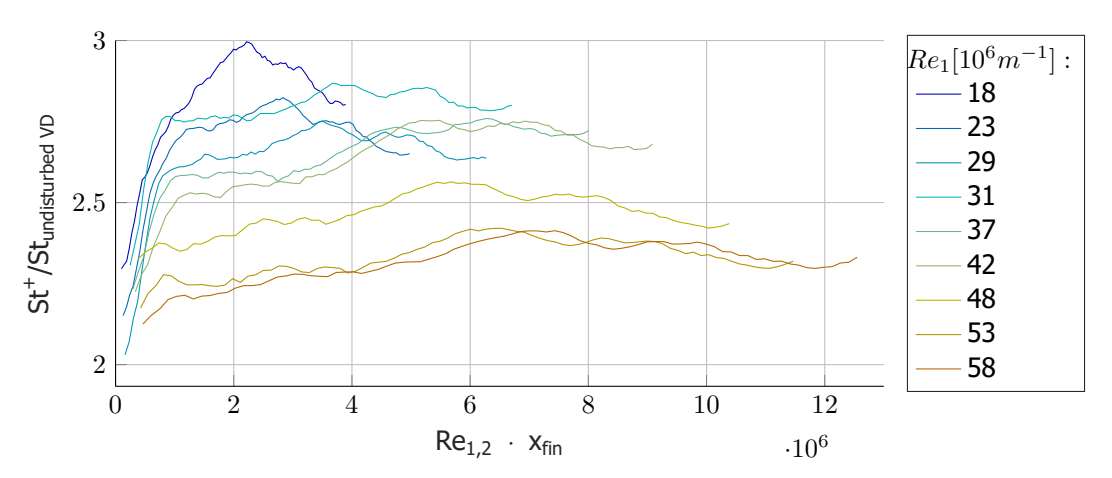


**Fig 12.** Scaled Stanton number ratios  $(St^+/St_{VD})$  along the reattachment line for the blunt fin with r=0.8 mm at various unit Reynolds numbers.

# 4. Conclusion

The surface heat flux in the vicinity of a single fin on a flat plate was investigated by quantitative infrared thermography (QIRT) for both a turbulent and a transitional boundary layer. This model geometry features a typical quasiconical separation vortex and very high heat loads near the reattachment line, that still cannot be sufficiently modeled or predicted with the currently available datasets or tools. With numerous experimental configurations, this study aimed to find scaling laws for this maximum heat load at the reattachment line of the separated flow, depending on the Mach number, the shock intensity and the state of the boundary layer.

From the experiments with a turbulent boundary layer, a correlation was derived to predict the rise in heat flux respective to the undisturbed boundary layer, depending on the shock intensity. The empirical dependencies of maximum heat loads on shock intensity in fully turbulent flows differed for the two investigated Mach numbers (M=3 and M=5), resulting in slightly different correlations. At high shock intensities with a fin angle of  $\beta \geq 26^{\circ}$ , the experimental Stanton number ration did not further rise and the found scaling laws loose their validity. This effect was related to a large scale 3D separation and the breaking of the quasiconical flow symmetry.

For transitional boundary layers, the progression of the Stanton number along the reattachment line was investigated in further detail. It was found, that a virtual, shortened boundary layer is suited for the scaling, that starts at the leading edge of the fin. Normalizing both the position and the rise in heat flux with this reference curve without shock, the quasiconical properties of the heat flux become revealed. Along the reattachment line, the normalized Stanton number increases but reaches a plateau value downstream of the effects of laminar-turbulent transition and the inception region. The level reached depends on the boundary layer state and could be scaled with the state parameter  $\zeta$  of the transitional boundary layer at the leading edge of the fin. The found linear trend for transitional boundary layers continues for a laminar boundary layer but not anymore for a fully turbulent one.

Within the parameter range of this study, the given equations suggest a fairly easy prediction of the maximum heat flux at a single fin on a flat plate. First, the Stanton number ratio for a turbulent boundary layer needs to be calculated with Eq. 4 or 5 from the Mach number and shock intensity. For a transitional boundary layer, that value is increased regarding Eq. 7. Next, the Stanton number level for an undisturbed boundary layer must be predicted by applying the Van Driest II method alongside the Reynolds analogy relation. Last, Eq. 2 needs to be inverted to calculate the expected heat flux on the model surface.

Nevertheless, it is reasonable to assume that such predictions based on correlations only apply to shock intensities and Mach numbers that have been studied. In order to rule out the influence of testing techniques and verify or adjust the proposed correlations, the effect of the transitional boundary layer on shock-induced thermal loads should be investigated as broadly as possible. Furthermore, studies on SBLI for boundary layers with  $\zeta < -0.4$  and  $\zeta > 1$  would greatly contribute to a comprehensive investigation of the effects of the boundary layer state and the limits of the obtained relationships.

#### References

- [1] J. Fang, Y. Yao, A.A. Zhelzovodov, and L. Lu. Investigation of three-dimensional shock wave/turbulent-boundary-layer interaction initiated by a single fin. <u>AIAA Journal</u>, 55:509–523, 2017.
- [2] E. Schülein. Skin-friction and heat flux measurements in shock/boundary-layer interaction flows. AIAA Journal, 44:1732–1741, 2006.
- [3] H. Babinsky and J.K. Harvey. <u>Shock Wave-boundary-layer Interactions</u>. Cambridge Aerospace Series, 2011.
- [4] Wieland Lühder. Messung der Wandschubspannung in Strömungen mit Stoß-Grenzschicht-Wechselwirkungen. PhD thesis, University Goettingen Repository, 2024.
- [5] H. Ludwieg. Der Rohrwindkanal. Zeitschrift für Flugwissenschaften, 3, 1955.
- [6] J. Lunte. <u>Stoßinduzierte Strömungsablösung in transitionellen Grenzschichten</u>. PhD thesis, Georg-Ausgust Universität Göttingen, 2021.
- [7] E. Schülein. Effects of laminar-turbulent transition on the shock-wave/boundary-layer interaction. In 44th AIAA Fluid Dynamics Conference, 2014.
- [8] Patrice Touré. <u>Turbulente Stoß-Grenzschicht-Wechselwirkungen durch laufende</u> Verdichtungsstöße. PhD thesis, TU Braunschweig, 2022.
- [9] D. L. Schultz and T. V. Jones. Heat-transfer measurements in short-duration hypersonic facilities. AGARD, 165, 1973.
- [10] F. White. Viscous Fluid Flow. McGraw-HiII, 2 edition, 1991.
- [11] M. Zhang, W. Si, and C. Lee. Heat transfer and recovery factor of aerodynamic heating on a flared cone. AIAA Journal, 59:4284–4292, 2021.
- [12] F. Alvi and G. Settles. Structure of swept shock wave/boundary-layer interactions using conical shadowgraphy. In 21st Fluid Dynamics, Plasma Dynamics and Lasers Conference, 1990.
- [13] Michael C. Adler and Datta V. Gaitonde. Flow similarity in strong swept-shock/turbulent-boundary-layer interactions. AIAA Journal, 57:1579–1593, 2019.
- [14] A. Baldwin, L.J. Mears, F.S. Alvi, R. Kumar, and J.W. Naughton. Effect of swept shockwave boundary-layer interaction strength on surface skin friction. AIAA Journal, 61:1608–1622, 2023.
- [15] G.S. Settles. Swept shock/boundary-layer interactions scaling laws, flowfield structure, and experimental methods. AGARD, 792:1–40, 1993.
- [16] E Reginald Van Driest. <u>The problem of aerodynamic heating</u>. Institute of the Aeronautical Sciences Los Angeles, 1956.
- [17] B. J. Abu-Ghannam and R. Shaw. Natural transition of boundary layers—the effects of turbulence, pressure gradient, and flow history. <u>Journal of Mechanical Engineering Science</u>, 22(5):213–228, October 1980.